Title

Increased Expression of Beige/Brown Adipose Markers from Host and Breast Cancer Cells Influence Xenograft Formation in Mice

Journal

Molecular Cancer Research, 14(1)

ISSN

1541-7786

Authors

Singh, Rajan
Parveen, Meher
Basgen, John M
et al.

Publication Date

2016

DOI

10.1158/1541-7786.mcr-15-0151

Peer reviewed

HHS Public Access

Author manuscript

Mol Cancer Res. Author manuscript; available in PMC 2017 January 01.

Published in final edited form as:

Mol Cancer Res. 2016 January ; 14(1): 78–92. doi:10.1158/1541-7786.MCR-15-0151.

Increased expression of Beige/Brown adipose markers from host and breast cancer cells influence xenograft formation in mice

Rajan Singh[1,2,3,††], **Meher Parveen**[1,††], **John M. Basgen**[1], **Sayeda Fazel**[1], **Meron F. Meshesha**[1], **Easter C. Thames**[4], **Brandis Moore**[1], **Luis Martinez**[1], **Carolyn B. Howard**[5], **Laurent Vergnes**[6], **Karen Reue**[6], and **Shehla Pervin**[1,2,3,*]

[1]Charles R. Drew University of Medicine and Science, Los Angeles, CA 90059, USA

[2]Department of Obstetrics and Gynecology, David Geffen School of Medicine at UCLA, Los Angeles, CA 90095, USA

[3]Jonsson Comprehensive Cancer Center at UCLA, Los Angeles, CA 90095, USA

[4]Columbia University, New York, NY 10027, USA

[5]Jackson State University, Jackson, MS 39217

[6]Department of Human Genetics, David Geffen School of Medicine at UCLA, Los Angeles, CA, 90095. USA

Abstract

The initiation and progression of breast cancer is a complex process that is influenced by heterogeneous cell populations within the tumor microenvironment (TME). Although adipocytes have been shown to promote breast cancer development, adipocyte characteristics involved in this process remain poorly understood. In this study, we demonstrate enrichment of beige/brown adipose markers, contributed from the host as well as tumor cells, in the xenografts from breast cancer cell lines. In addition to uncoupling protein-1 (UCP1) that is exclusively expressed in beige/brown adipocytes, gene expression for classical brown (MYF5, EVA1 and OPLAH), as well as beige (CD137/TNFRSF9 and TBX1) adipocyte markers, were also elevated in the xenografts.

[*]Corresponding Author: Shehla Pervin, Division of Endocrinology and Metabolism, 1731 East 120th Street, Charles R Drew University of Medicine and Science, Los Angeles, CA 90059. Phone: 323-563-9342; shehlapervin@cdrewu.edu, spervin@mednet.ucla.edu.

[††]These authors contributed equally.

Disclosure of Potential Conflicts of Interest

The authors do not have any potential conflicts of interest.

Author's Contributions

Conception and design: R. Singh, S. Pervin

Development of methodology: S. Pervin, J.M. Basgen, S. Fazel, E.C. Thames, L. Vergnes, R. Singh

Acquisition of data: R. Singh, M. Parveen, J.M. Basgen, S. Fazel, M.F. Meshesha, E.C. Thames, B. Moore, L. Martinez, L. Vergnes, S. Pervin

Analysis and interpretation of data: R. Singh, M. Parveen, J.M. Basgen, L. Vergnes, K. Reue, S. Pervin

Writing and review of the manuscript: R. Singh, J.M. Basgen, L. Vergnes, K. Reue, S. Pervin

Administrative, technical and material support: R. Singh, M. Parveen, J.M. Basgen, S. Fazel, M.F. Meshesha, E.C. Thames, B. Moore, C.B. Howard, L. Martinez, L. Vergnes, S. Pervin

Study supervision: R. Singh, S. Pervin

Enrichment of beige/brown characteristics in the xenografts was independent of the site of implantation of the breast tumor cells. Early stages of xenografts showed an expansion of a subset of mammary cancer stem cells (MCSCs) that expressed PRDM16, a master regulator of brown adipocyte differentiation. Depletion of $UCP1^+$ or $Myf5^+$ cells significantly reduced tumor development. There was increased COX-2 (MT-CO2) expression, which is known to stimulate formation of beige adipocytes in early xenografts and treatment with a COX-2 inhibitor (SC236) reduced tumor growth. By contrast, treatment with factors that induce brown adipocyte differentiation *in vitro* led to larger tumors *in vivo*. A panel of xenografts derived from established breast tumor cells as well as patient-tumor tissues were generated that expressed key brown adipose tissue (BAT)-related markers and contained cells that morphologically resembled brown adipocytes.

Implications—This is the first report demonstrating that beige /brown adipocyte characteristics could play an important role in breast tumor development and suggest a potential target for therapeutic drug design.

Introduction

Breast cancer remains the second leading cause of death in women (1). Persisting high mortality rate warrants deeper understanding of this complex disease. Breast tumors are composed of heterogeneous cell populations, some of which have stem cell-like properties that enable them to resist most therapeutic treatments (2). It is known that adipose rich microenvironment of mammary glands, which is composed of mature adipocytes and adipose-derived stem cells (ADSCs), dynamically influence breast tumor development (3, 4). Cancer cells are also reported to induce lipolysis of adipocytes where free fatty acids have been known to accumulate in cancer cells and promote its growth (5). In addition, adipocytes in the vicinity of breast tumor cells exhibit altered biological characteristics such as over-expression of inflammatory cytokines, proteases, and collagens that are involved in remodeling of extracellular matrix (6). Some of these properties are acquired due to breast tumor cells secreting pro-inflammatory interleukin-6 (IL-6) and Wnt3a that reactivates Wnt/β-catenin pathways in adipocytes to form adipocyte-derived fibroblasts (ADF) (7). In return, these ADF and cancer-associated adipocytes (CAA) increase aggressive tumor behavior like invasiveness and angiogenesis (7, 8).

Mammary adipose tissue also provides a reservoir of mesenchymal stem/progenitor cells or ADSCs that are recruited to the tumor mass in response to inflammation and hypoxic conditions (9). These resident ADSCs, as well as recruited bone-marrow derived mesenchymal stem cells (BM-MSCs), constitute the mammary cancer stem cell (MCSC) populations that play a key role in promoting the initiation/progression of breast cancer (10). Interestingly, breast-derived adipose stromal cells express significantly increased levels of genes implicated in cell growth, matrix deposition, remodeling and angiogenesis when compared to BM-MSCs, which have previously been implicated in breast tumor development (9). In particular, ADSCs induce epithelial to mesenchymal transition (EMT) in a PDGF-dependent manner (11).

Although several lines of evidence have implicated white adipocytes in promoting aggressive breast tumor behavior, a few recent studies have also associated brown adipocytes with this complex disease (12, 13). Brown adipose tissue (BAT) has also been detected in postnatal mammary gland along with white adipocytes (14). In spite of significant involvement of adipose tissue in progression of breast tumors, specific adipocyte characteristics that promote breast tumor development remain poorly understood. Identification and characterization of key players involved in early stages of tumor development could lead to effective therapeutic intervention to control breast cancer. This report provides significant evidence that expression of beige and brown adipose markers from host and tumor cells could influence breast tumor growth in nude mice. Therefore, therapeutic targeting of BAT has the potential of yielding beneficial effects for the treatment of breast cancer.

Materials and Methods

Human Cell Lines

The HMLE^{HRASV12} cell line, obtained after transforming HMLE (human mammary epithelial) cells with HRAS T24 oncogene was obtained in 2011 from Robert Weinberg (Whitehead Institute, Cambridge, MA) (15) and cultured in DMEM-F12 containing 10% FBS. Human breast cancer cell lines MDA-MB-231 and MDA-MB-468 were obtained from American Type Culture Collection (ATCC) (Manassas, VA) in 2013. ATCC uses Promega PowerPlex 1.2 system and the Applied Biosystems Genotyper 2.0 software for analysis of amplicon. We have not done any further testing in our lab. MDA-MB-231 was propagated in Leibovitz's L-15 medium containing 10% FBS. MDA-MB-468 was propagated in RPMI 1640 containing 10% FBS as before (16).

Xenograft formation

Six to eight week old nude mice (Harlan Laboratories Inc. Indianapolis, IN) were implanted subcutaneously (posterior dorsolateral) with HMLE^{HRASV12}, MDA-MB-468 and MDA-MB-231 cells (2×10^6 cells/100μl) mixed with matrigel (1:1). To generate transplantable xenografts, primary xenografts were dissociated with 0.2% collagenase (type IV, Sigma Aldrich, St. Louis, MO) for 1hr at 37°C, propagated for 48h *in vitro* and implanted (1×10^6 cells/injection) in nude mice. For some experiments, the cells were implanted at various subcutaneous sites like posterior ventral, anterior ventral and anterior dorsolateral. Tumors were excised at various time points and tumor weight was measured. In some cases, tumor volume was calculated as described previously (17, 18). This study was carried out in strict accordance with the recommendations in the Guide for the Care and Use of Laboratory Animals of the National Institutes of Health. The protocol was approved by the Institutional Animal Care and Use Committee on the Ethics of Animal Experiments of the Charles R. Drew University of Medicine and Science (permit number: I-1103-261).

Histology

Immediately after excision from mice, tumors were placed in 2.5% glutaraldehyde in Millonig buffer. After 24 hours fixation tumors were washed three times with Millonig buffer for two hours and post-fixed in 1% osmium tetroxide for one hour. Osmium tetroxide

crosslinks lipids and prevents loss of cytoplasmic lipid during subsequent tissue dehydration. Osmium tetroxide also stains lipid droplets brown (19). Following three additional two-hour washes with buffer, the tumors were dehydrated with 70%, 90%, 95%, and 100% ethanol, and embedded in glycol methacrylate (Kulzer Technovit 7100, Electron Microscopy Sciences, Hatfield, PA) according to the manufacturer's protocol. From the methacrylate blocks, five-micrometer thick sections were cut using a RM2255 microtome (Leica Microsystems, Buffalo Grove, IL), placed on glass slides, dried on a hotplate, and stained with 0.5% toluidine blue. Images were obtained using a standard Olympus BX51 bright field microscope with a DP-71 digital camera and DP Controller software (Olympus America, Cypress, CA).

Quantitation of lipids in cross-section of xenografts

To quantify the amount of lipids (including triglycerides) present in tumor cross section, the blob algorithm was used (20). Using MATLAB, the images of the osmium tetroxide and toluidine-stained tissue sections were converted from RGBA to grayscale and processed; histogram equalization was used to enhance the contrast in the images for better differentiation between tumor structures and low pass filtering was utilized to reduce pixilation. Then, blob analysis was performed, a process in which pixels whose intensity values (0 as black and 256 as white in image class uint8 or 8-bit image) fall within a specified range are retained as 1's in a binary image and those outside of the range are converted to 0's, and connected pixels whose values are 1's are grouped and labeled. Osmium tetroxide fixation makes lipid regions distinguishable from other tumor tissues because the osmium tetroxide stains lipid droplets brown, so pixels that depict these regions are of generally lower intensities than those of other tissues. The areas of the labeled groups are then calculated and the original image and blob-analyzed image are compared to determine which areas are truly areas containing high amounts of lipids. For each tumor section image, two pixel intensity ranges are used separately to obtain the total tumor section area and the total area of regions containing high amounts of lipids.

Immunolabeling

Immediately after excision from mice, some of the tumors were fixed in 5% formalin overnight after which they were dehydrated in ethanol and embedded in paraffin. Tumor sections (5–6μm) were deparafinized, and immunolabeling was performed as described previously (21). Cells from dissociated $HMLE^{HRASV12}$ xenografts (both transplantable and non-transplantable) were plated in six well plates and allowed to propagate for 48 hrs. Cells were fixed with 4% paraformaldehyde in 1× PBS for 30 min, washed, and incubated with blocking buffer (TBS pH 7.8, 5% normal goat serum, 1% BSA and 1% triton X-100) for 1hr. The following antibodies were used in our experiments: UCP1 (ab10983, Abcam), UCP2 (AB3226, Millipore, Billerica, MA); and UCP3 (ab3477, Abcam).

Quantitative Real-Time PCR

Total RNA isolated from flash-frozen xenografts or cells were subjected to reverse transcription, and the resulting cDNA was analyzed for various gene expression by real-time quantitative PCR using a 7500 Fast Real-time PCR System (Applied Bio Systems, Foster City, CA) and associated software as described before (21, 22). Human or mouse primer sets

(Supplementary Table 1) were designed using Primer Bank DNA Core Facility (http://pga.mgh.harvard.edu/primerbank) (MGH Harvard, Cambridge, MA) (22, 23).

Western blots Analysis

Xenografts at various time points were lysed and 75 μg of total protein was resolved on 4–15% SDS-PAGE gels and electro-transferred to polyvinylidene difluoride (PVDF) membranes as described previously (18, 19). The membranes were incubated with the following primary antibodies at 1:1000 dilutions: UCP1 (ab10983, Abcam), UCP2 (AB3226, Millipore, Billerica, MA), UCP3 (ab3477, Abcam, Cambridge, MA), PRDM16 (sc130243, Santa Cruz Biotech, Dallas, TX), PGC-1α (sc-13067, Santa Cruz Biotech, CA), C/EBP-α (sc-16, Santa Cruz Biotech, Dallas, TX), PPARγ (sc-7273, Santa Cruz Biotech, Dallas, TX), COX IV (ab14744, Abcam, Cambridge, MA), COX-2 (160112, Cayman Chemicals, Ann Arbor, MI), ALDH1 (611195, BD Transduction, San Jose, CA), CD44 (3570S, Cell Signaling, Beverly, MA), Myf5 (sc-302, Santa Cruz Biotech, Dallas, TX); CD137 (ab3169, Abcam, Cambridge, MA), p38 MAPK (9212S, Cell Signaling, Beverly, MA), VEGF (ab46154, Abcam, Cambridge, MA), Cyclin D1 (sc 717, Santa Cruz Biotech, Dallas, TX), ColA1 (sc 25974, Santa Cruz Biotech, Dallas, TX), α-SMA (sc 53142, Santa Cruz Biotech, Dallas, TX), FN (HFN 7.1, Hybridoma Bank, Iowa City, IA), pp38 MAPK (9211S, Cell Signaling, Beverly, MA), and β-actin (sc-81178, Santa Cruz Biotech, Dallas, TX).

Flow Cytometry

Cells from dissociated xenografts were incubated with anti-UCP1, UCP3 (1:100 dilution), Myf5 (1:50 dilution), or PRDM16 (1:50 dilution) antibodies for 1 hr at room temperature. Cells were further incubated with FITC or Texas-Red conjugated secondary antibodies (Vector Laboratories) at 1:200 dilutions for 40 minutes. The ALDEFLUOR kit (StemCell Technologies, Durham, NC) was used to isolate the population with high ALDH1 enzymatic activity as described before (18). To distinguish between ALDH1+ and ALDH1− cells, a fraction of cells were incubated under identical conditions in the presence of a 10-fold molar excess of the ALDH1 inhibitor, diethylaminobenzaldehyde (DEAB). UCP1+, ALDH1+, and Myf5+ cell populations were sorted in a BD FACS Aria II high speed cell sorter (Becton Dickinson, Palo Alto, CA, USA) (18).

Double Immunofluorescence

Dissociated cells obtained from the xenografts were analyzed for co-localization of extracellular matrix proteins and adiponectin (Adipoq) with UCP1 using previously described methods (21). Briefly, dissociated cells were seeded overnight on eight well chamber slides, fixed with 2% paraformaldehyde, blocked with normal goat serum containing 0.25% Triton X100. Cells were initially incubated with anti-UCP1 antibody followed by FITC (for co-localization with extra-cellular matrix proteins) or Texas-Red (for co-localization with adiponectin) conjugated secondary antibodies. Subsequently, the cells were further incubated with anti-ColA1, -Col3, -α-SMA, and FN or adiponectin followed by appropriate Texas-Red or FITC conjugated secondary antibodies for 1hr. Slides were further counterstained with DAPI and mounted in prolong anti-fade solution (Molecular Probes, Eugene, OR) (21).

Cellular Oxygen Consumption

Oxygen consumption rates (OCR) of single cell suspensions obtained from 7- and 12- week xenografts were measured in an XF24 Extracellular Flux Analyzer (Seahorse Bioscience, North Billerica, MA, USA). Cells (4×10^4/well) were plated in DMEM containing 10% FBS and incubated overnight at 37°C with 5% CO_2. The day of the assay, medium was replaced by un-buffered DMEM supplemented with 25 mM glucose, and cells were incubated at 37°C in a CO_2-free incubator for 2 hr before oxygen consumption rate (OCR) was recorded. During the assay, 0.5 μM carbonyl cyanide-p-trifluoromethoxyphenylhydrazone (FCCP) was injected to deduce the maximal respiration capacity (23, 24).

Human Tumors

Human tumor samples were obtained from the Cooperative Human Tissue Network (CHTN) (http://chtn.nci.nih.gov) and National Disease Research Institute (NDRI) (http://ndriresourse.org). Studies were performed under research protocol approved by the Charles R. Drew University of Medicine and Science Institutional Review Board (permit number: 09-08-2229-06).

Statistical Analysis

Data are presented as mean ± SD, and differences between groups were analyzed using ANOVA. If the overall ANOVA revealed significant differences, then pair-wise comparisons between groups were performed by Newman-Keuls multiple group test. All comparisons were two-tailed and $p<.05$ were considered statistically significant. The experiments were repeated at least three times, and data from representative experiments are shown.

Results

Increased beige/brown adipocyte characteristics in xenografts from HMLE^{HRASV12} cells

To identify specific cell types that promote breast tumor initiation, we enriched for actively tumorigenic cells by generating transplantable xenografts derived from HMLE^{HRASV12} cells. Transplantable xenografts were generated by a round of *in vitro* culturing of cells from primary xenografts for 48h and further implanting them subcutaneously *in vivo* at a posterior dorsolateral site in the host. We obtained two classes of xenografts: those that could be transplanted with approximately 95% efficiency (transplantable, T), and others that did not grow or gave rise to cystic tumors (non-transplantable, NT) (Supplementary Fig. S1A). Even though most of the T tumors grew as a solid mass, there was variability in their morphology and growth kinetics. However, most of these T tumors when dissociated appeared to contain adipocyte-like cell. Paraffin-embedded cross sections of HMLE^{HRASV12} xenografts were stained with eosin/hematoxyin to examine the general morphology of these tumors. We found significant lipid filled cells surrounding and invading the tumor mass in these xenografts (Figure 1A–C). In order to preserve the lipid content within the xenografts (5–7 weeks), tissues were fixed with glutaraldehyde and post-fixed with osmium tetroxide that stains and cross-links lipid droplets. A systematic analysis revealed that only T tumors contained cells with multi-locular lipid droplets, a morphology that is characteristic of beige/

brown adipocytes (Fig. 1D–E, Supplementary Fig. S1.B). A quantitative analysis of lipids including triglycerides was performed in cross section of osmium tetroxide infiltrated xenografts (5 week) using blob algorithm with MATLAB software as explained in the Method Section. We have analyzed 3 xenografts (4 sections from each xenograft) and found variations (2–6%) in the total area occupied by lipids in the cross-section of respective xenografts. Quantitation from one of the xenografts analyzed is shown (Supplementary Fig. S1C). Cells cultured from dissociated T xenografts stained positive for uncoupling protein 1 (UCP1), which is predominantly expressed only in beige and brown adipocytes (25) (Supplementary Fig. S1D). In addition, cells from these xenografts also stained for UCP2, and UCP3, whereas cells from NT tumors were negative for these uncoupling proteins (Supplementary Fig. S1D). We further immunolabeled paraffin embedded sections of xenografts from $HMLE^{HRASV12}$ for UCP1 and these immunolabeling experiments showed that lipid-filled cells expressed UCP1 protein (Fig. 1F). In addition to the uncoupling proteins, we analyzed the expression levels of Prdm16, a master regulator of brown fat lineage and Pgc1, a transcriptional coactivator of Prdm16 expressed in brown adipocytes (26, 27). We also examined in the xenografts, the expression of Cebpa, and Pparg, which are key transcription factors promoting adipogenesis (24). Quantitative PCR analysis of T tumors (5 weeks) using human specific primers showed significantly increased expression of key brown adipose specific markers including Ucp1 (12.5±2.7 fold), Ucp3 (7.4±1.8 fold); Prdm16, (4.7±1.2 fold), Pgc1 (3.4±0.9 fold), Cebpa (5.8±1.4 fold), and Pparg (2.7±0.8 fold) (Fig 1G) (25, 26). It has been reported Ucp1 and Prdm16 are expressed in both inducible beige (which originates from non-Myf5 WAT), as well as in classical brown adipocytes (which originate from Myf5-expressing progenitor populations) (28). Gene expression levels for additional markers characteristic of both beige adipocytes such as Cd137 (3.7±0.5 fold); and Tbx1 (4.4±1.2 fold) as well as classical brown adipocytes including Myf5 (3.4±0.7 fold); Eva1 (2.4±0.6 fold); Oplah (6.3±1.3 fold) and Lhx8 (14.4±3.2 fold) were also significantly elevated in T but not in NT tumors (Fig. 1H). Zeb2, which is associated with aggressive tumor behavior (29) including epithelial to mesenchymal transition (EMT) was significantly increased (4.6±0.7 fold) only in T xenografts (Fig. 1G). Increased protein levels of UCP1, UCP3, PRDM16, Myf5, adipocyte-specific transcription factors PGC-1α and PPARγ were also found in T tumors when compared to NT (Fig. 1I). These data shows the expression of beige and brown adipose markers in transplantable xenografts from $HMLE^{HRASV12}$.

Both tumor cells and host contribute to the increase in beige/brown adipose markers $HMLE^{HRASV12}$ xenografts

Since host microenvironment is known to significantly contribute to tumor progression (30), we further set out to distinguish the contribution of the host as well as the implanted tumor cells themselves for the expression of beige/brown adipose markers in xenografts. For this purpose, primers designed from human (h) and mouse (m) Ucp1 and Prdm16 (beige/brown adipocytes), Cd137 and Tbx1 (beige adipocytes) as well as Myf5, Eva1 and Oplah1 (classical brown adipocytes) genes were tested for species specificity. Species specificity of each of the primer pairs was pre-determined by its ability to amplify respective genes from known specific tissues that overexpress them (Supplementary Fig. S2). Mouse brown adipose tissue (BAT) that is known to have increased expression of Ucp1, and Prdm16 was

used as a positive control for mouse primers (Supplementary Fig. S2). Human peri-adrenal adipose tissues from pheochromocytoma patients, which are known to be enriched in beige/brown adipocytes (31), were used as a positive control to determine the specificity of human primers. Only those mouse or human primer sequences (Table 1) that amplified specific genes from either BAT (Ct= 15–25) or human tumors (Ct =22–30) respectively were subsequently used in this study (Supplementary Fig. S2). A difference of five Ct (which represent more than 32-fold difference) between mouse and human primers was considered specific (Fig S2). While using human and mouse primers to amplify peri-adrenal adipose tissues cDNA template, we obtained following differences (human vs. mouse) in their Ct values- Ucp1:~24 vs. ~40; Cd137:~30 vs. ~38; Myf5:~34 vs. ~42; Prdm16:~34 vs. ~42; Oplah: ~30 vs. ~36; Eva1:~26 vs. ~34, and Tbx1:~31 vs. ~40. Similarly, while using mouse and human primers to amplify mouse BAT cDNA template, we obtained following differences (mouse vs. human) in their Ct values- Ucp1:~17 vs. ~37; Cd137:~32 vs. ~36; Myf5:~26 vs. ~36; Prdm16:~26 vs. ~37; Oplah: ~26 vs. ~34; Eva1:~24 vs. ~34, and Tbx1:~28 vs. ~32. Our data, therefore, suggest specificity of species-specific primer sets used for this study.

$HMLE^{HRASV12}$ xenografts (3–5 weeks) were excised after growth at a subcutaneous site (posterior dorsolateral) and examined for expression of beige and brown adipocyte markers using respective human and mouse specific primers. When compared to $HMLE^{HRASV12}$cells (before implantation), there was increased expression of hUCP1 (10.8±1.9 fold), hPRDM16 (2.8±0.7 fold), hCD137 (2.5±0.8 fold), hTBX1 (3.5±0.6 fold), hMYF5 (7.2±2.1 fold), hEVA1 (2.2±0.13 fold), and hOPLAH (5.4±1.3 fold) in the xenografts (Fig. 1J). In addition, when compared to the basal expression in the host tissues at the site of implantation (posterior dorsolateral) there was significantly increased expression of mUcp1 (11.4±1.2 fold), mPrdm16 (3.1±0.7 fold), mCd137 (11.8±1.6 fold), and mTbx1 (12.4±1.7 fold) in the xenografts (Fig. 1K). No significant expression of mouse Myf5, Eva1 or Oplah was observed in the xenografts analyzed. Our data, therefore, suggests beige adipose markers of host origin in the $HMLE^{HRASV12}$ xenografts as analyzed by the expression of CD137 and Tbx1. Also our data indicates that human breast tumor cells expressed key adipose markers in xenografts.

Increase in beige/brown adipose markers in xenografts was independent of the site of implantation of $HMLE^{HRASV12}$ cells

Human breast tumors have been found to recruit mesenchymal stem cells as well as adipocytes from its immediate microenvironment and distant sites of the host (10, 30). We therefore, next examined the possibility whether recruitment from the host microenvironment, in part contributed to increased expression of beige/brown adipose markers detected in the $HMLE^{HRASV12}$ xenografts. For this purpose, we initially examined the basal expression of mUcp1, mPrdm16, mCd137 and mMyf5 at various sites in a control host where no tumor cells were implanted. Significant mUcp1 (Ct=17–18), mMyf 5 (Ct=29) and mPrdm16 (Ct =33) expression was detected specifically in the interscapular tissues of the host, which is a known depot of brown adipocytes. Some mUcp1 (Ct=27) and mMyf 5 (Ct=30) expression was detected in the abdominal (ventral posterior) subcutaneous adipose tissue scrapped from the host. No significant expression of mUcp1, mPrdm16 and mMyf5

was detected in the inguinal or thoracic mammary glands, or subcutaneous adipose tissue from the posterior dorsal or dorsolateral region of the host. A basal expression of mCD137 (Ct=30–31) was detected in most of the host tissues examined. No significant expression with hUcp1, hPrdm16, hCD137 and hMyf5 was detected in any of the host tissues examined.

We further examined whether site of implantation of the HMLE^{HRASV12} tumor cells contributed to the increase of beige/brown adipocytes in the xenografts. Since xenografts from a subcutaneous site (posterior dorso-lateral) had significantly increased beige/brown adipocytes, we further implanted the tumor cells at three different subcutaneous sites including posterior ventral, posterior ventrolateral and anterior dorsal of the host. When tumor cells were implanted at posterior ventrolateral site of the host, xenografts (3–5 week) had significantly increased expression of various beige and brown adipose specific markers. When compared to HMLE^{HRASV12}cells (before implantation), there was increased contribution of beige/brown adipose markers from tumor cells (hUcp1: 11.4±2.2; hCd137: 3.7±0.6; hTbx1: 4.2±0.5; hMyf5: 5.5±0.14; hEva1: 2.1±0.11) in the xenografts. In addition, when compared to control host tissues at posterior ventrolateral site, there was increase host contribution of these markers (mUcp1: 14.2±1.2; mCd137: 14.4±2.7; and mTbx1: 12.8±1.8) in the xenografts (Supplementary Fig. S3). Similar changes were found when these cells were implanted at other subcutaneous sites (Supplementary Fig. S3). We also injected tumor cells in the inguinal mammary glands of the host and found similar increase in beige/brown adipose markers in the xenografts (data not shown). These experiments suggest that increased expression of beige and brown adipose markers in the HMLE^{HRASV12} xenografts was independent of the site of implantation of the tumor cells.

Temporal regulation of UCP1 expression during xenograft development

We further examined morphological characteristics as well as the expression of various proteins associated with beige/brown adipose during the course (1–15 week) of xenograft development. Morphological characteristics were examined in formalin-fixed HMLE^{HRASV12} xenografts that were infiltrated with osmium and embedded in paraffin. Representative pictures (low and high magnification) of eosin/hematoxylin stained xenograft (5 week) is shown (Fig. 2 A–B). We further performed western blot analysis of pooled tumor samples at intervals from 1–15 weeks, which revealed a dynamic pattern of UCP1 expression during tumorigenesis (Fig. 2C–D). The levels of UCP1 and UCP3 proteins were temporally regulated during tumorigenesis, with peak levels at weeks 5–7 for UCP1 and UCP3 (Fig. 2D). PRDM16 levels were increased as early as 1 week after implantation of the cells while Myf5 peaked between 3–5 weeks of tumorigenesis. On the other hand, increased levels of CD137 were detected as early as 1 week of implantation of HMLE^{HRASV12} cells. Also, COX IV, a mitochondrial protein, as well as PGC-1α, PPARγ and C/EBP-α followed dynamics similar to UCP1, peaking at the middle stages of tumor growth (Fig. 2D). UCP2 expression was detected only in late stage tumors (Fig. 2D). Quantification by fluorescence activated cell sorting (FACS) confirmed increased PRDM16 (7.8% and 3.6%) expression in weeks 1 and 3 respectively in addition to increase in UCP1 (0.2% and 6.8%) and UCP3 (0.1% and 1.6%) from week 1 to 5 respectively (Fig. 2E). Since xenografts that contained beige/brown adipose exhibited a growth advantage over NT xenografts, we examined

expression of aggressive tumor markers in these tumors. The levels of vascular endothelial growth factor (VEGF), proliferation marker, cyclin D1 as well as extracellular matrix proteins, collagen A1 (ColA1), smooth muscle actin (SMA) and fibronectin (FN) were assessed by Western blot, We found increased levels of VEGF, cyclin D1, ColA1, SMA and FN in T tumors when compared to NT (Fig. 2F). We further examined the presence of extracellular matrix proteins with UCP1 expression in sections of T xenografts by double immunofluorescence. We found extracellular matrix proteins in close proximity to UCP1-expressing cells in the xenografts (Supplementary Fig. S4A). We further examined whether UCP1-expressing cells also expressed adiponectin, which is highly expressed in adipocytes. Cells from dissociated xenografts were fixed and stained for UCP1 (Texas Red) and adiponectin (FITC). We found UCP1-expressing cells also co-expressed adiponectin and a representative picture is shown (Supplementary Fig. S4B). Since brown adipocytes are significantly enriched in mitochondria, we analyzed the cellular bioenergetics of cells from 7 (early-mid stage) and 15 week (late stage) xenografts. Cellular respiration was measured in basal and after sequential injection of the ATP synthase inhibitor oligomycin, the uncoupling agent FCCP and the mitochondrial inhibitors rotenone and myxothiazol, allowing the calculation of different mitochondrial respiration parameters. Seven week xenograft-derived cells exhibited higher oxygen consumption rates (OCR) of mitochondrial (20.1±1.3 vs. 5.5±0.7); ATP-linked (14.8±0.7 vs. 3.4±0.5); and maximal (34.9±3.0 vs. 10.6±1.5) respiration as well as proton leak (5.4±1.3 vs. 2.1±0.2) compared to 15 weeks (Fig. 2G). The increase in cellular bioenergetics was in agreement with the enhancement of mitochondrial protein expression observed at 5–7 weeks (i.e. UCP1 and COX IV in Fig. 2D). Our data, therefore, shows temporal regulation of beige and brown adipose specific proteins during $HMLE^{HRASV12}$ xenograft development.

Depletion of UCP1 and Myf5 positive population reduced xenograft development

Since increased brown and beige adipocyte characteristics were found only in transplantable xenografts, we further examined its role in breast tumor development. To assess functional differences between the UCP1+ cells present in early-stage tumors and UCP1-depleted ($UCP1^{-}$) cells that predominate in later stages, we tested the ability of each cell population to establish tumors *in vivo*. First, we compared tumor formation in nude mice after injection of the total cell population (2×10^6 cells) from 5-week xenografts to the $UCP1^{-}$ cell population (2×10^6 cells). At 10 weeks after injection, tumors from $UCP1^{-}$ cells had significantly attenuated growth (194.0±84.3 mg vs. 687.6±182.4 mg), (Fig. 3A). A second assay was based on the observed decline in UCP1 levels in late-stage xenografts (Fig. 2D). We assessed the potency of cells (2×10^6) from 7-week (high UCP1 levels) and 15-week (low UCP1 levels) xenografts to form tumors in mice, and observed that cells from 15-week xenografts produced delayed growth of tumors after 10 week (443.7±163.3 mg vs. 237.1±84.3 mg) and 15 week (875.5±213.2 mg vs. 355.8±103.4 mg) (Fig. 3B).

We next investigated whether PRDM16 expressing progenitor populations have a relationship to mammary cancer stem cells (MCSC), which have a key role in mammary tumor initiation and progression (32). The levels of aldehyde dehydrogenase 1 (ALDH1), a marker of MCSC, were highest in very early stage xenografts (7.4% of cells at 1 week) and subsequently declined (to 2.8% at 3 weeks) (Fig. 3C). We also detected the highest levels of

PRDM16 in very early stage xenografts (Fig. 2D), raising the possibility that a sub-population of MCSCs may also be expressing PRDM16. Consistent with this hypothesis, FACS analysis identified that 4.2% and 1.9% cells were positive for both ALDH1 and PRDM16 from 1-week and 3 week xenografts (Fig. 3C). We further examined Myf5 expressing cells in paraffin-embedded sections of xenografts by immunohistochemistry. A representative picture of Myf5 expression in undifferentiated cells in xenograft (3 week) is shown (Fig. 3D). For quantitation of Myf5 expressing cells in the xenografts, cells from dissociated xenografts were incubated with Myf5 antibody /FITC conjugated secondary antibody and subjected to FACS. While the % of Myf5 in the xenografts varied (0.2%–5.6%), a representative picture of cell sorting for Myf5 (2.7%) is shown (Fig. 3E). We further compared the potency of Myf5 depleted populations when compared to control cells in establishing xenografts. Analysis at 4 week showed that when compared to control cells (2×10^6), there was a lag in the Myf5-depleted (2×10^6) population to form xenografts (Fig. 3F). The above data suggests that UCP1 expressing beige/brown adipose along with Myf5 expressing cells contribute towards $HMLE^{HRASV12}$xenograft development.

Pre-treatment of $HMLE^{HRASV12}$ cells with brown adipocyte differentiation medium (BADM) increased beige adipocytes and xenograft growth

Since beige adipocytes, which could be induced, were present in the xenografts, we further examined the expression of inflammatory markers COX-2 and p38 MAP Kinase, both of which have been demonstrated to play key roles in promoting induction of beige adipocytes (33). COX-2 was expressed at highest levels at early stages of xenograft development (Fig. 4A), while the expression of phosphorylated p38 MAP Kinase followed dynamics (Fig. 4A) similar to that observed for UCP1 (Fig. 2D). Since cells from UCP1-enriched xenografts had growth advantage (Fig. 3B), we further examined whether deliberate inducement of beige adipocyte characteristics increased tumorigenic capacity. To test this, we stimulated primary cultures obtained from T xenografts with BADM containing 20nM insulin, 0.5 mM 3-isobutyl-1-methylxanthine (IBMX), 0.5μM dexamethasone, 0.125 mM indomethacin, and 1nM T3 (27) for 48 hrs and implanted induced and un-induced cells (2×10^6) subcutaneously (posterior ventrolateral site). Analysis of the xenografts (2 week) showed that beige adipocyte-specific markers contributed from both tumor cells and the host was significantly increased in the induced when compared to un-induced xenografts (Fig. 4B). We found increased expression of hUCP1 (1.8±0.4), hPRDM16 (2.4±0.2), hCD137 (2.7 ±0.02) and hTBX1 (1.8 ±0.38) as well as mUCP1 (4.7±0.7), mPrdm16 (2.8±0.2), mCd137 (6.5 ±0.4) and mTbx1 (7.2 ±0.1.8) in the induced when compared to un-induced xenografts (Fig. 4B). When the volumes of xenografts were examined, those from BADM-treatment generated larger tumors (949.8±154.6 mm^3) than those obtained from control cells (436.6±173.4 mg) after 4 weeks (Fig. 4C). Pretreatment of cells before implantation with 10nM SC236 (COX-2 inhibitor), prevented enhanced tumor growth (949.8±154.6 mm^3 vs. 519.8±183.4 mm^3), which was not observed when cells were pretreated with 10nM SC560 (COX-1 inhibitor) (Fig. 4C). Analysis of resulting tumors (2 weeks) obtained from BADM-induced (BADM+) showed increased protein levels of UCP1, UCP3, PRDM16, CD137, and COX-2 compared to the un-induced group (Fig. 4D). Furthermore, level of these proteins were significantly down-regulated in tumors obtained from cells injected after treatment with a combination of BADM+ and COX-2 inhibitor (SC236) compared to BADM+ group

alone (Fig. 4D). Our data shows stimulation of HMLE^{HRASV12} cells with BADM resulted in larger xenografts with increased beige adipocyte-specific markers when compared to un-induced xenografts.

Beige/brown adipocyte characteristics were found in xenografts from additional breast cancer cell lines

To determine whether increase of beige and brown adipocyte-like features is a common event in breast tumor development, we analyzed tumors from two additional breast cancer cell lines MDA-MB-468, and MDA-MB-231. Each of these cell lines (2×10^6 cells) were injected subcutaneously in the posterior dorsolateral side of nude mice for establishment of xenografts. In order to examine the adipose tissue surrounding or invading tumor mass, cross sections of 5 week MDA-MB-468 xenografts were stained with eosin/hematoxylin. A representative picture of these xenografts in low and high magnification is shown (Figure 5 A–C). In addition, 5 weeks xenografts from MDA-MB-468 and MDA-MB-231 were excised, fixed with glutaraldehyde, and post-fixed with osmium tetroxide. Histological analysis of the xenografts from each of these cell lines revealed multi-locular cells, characteristic of beige and brown adipocytes (Fig. 5G–H, Supplementary Fig. S4C). MDA-MB-468 (468) and MDA-MB-231 (231) xenografts were analyzed for expression levels of beige/brown adipocyte specific markers by quantitative PCR. Expression levels of hUCP1 (468: 7.5±1.1, 231: 9.7±2.1), hPRDM16 (468: 3.2±0.8, 231: 5.2±0.87), hCD137 (468: 4.1±1.5, 231: 2.4±0.4), hTBX1(468: 3.5±0.8, 231: 2.4±0.7), hMYF5 (468: 6.3±1.1, 231: 3.8±0.8), hEVA1(468: 1.7±0.5, 231: 1.2±0.3), hOPLAH (468: 4.2±0.4, 231: 2.4±0.2), were elevated in 5 week old xenografts from MDA-MB-468 (468), and MDA-MB-231 (231) breast cancer cell lines (Fig. 5D and 5I). Expression levels of mUcp1 (468: 14.5±3.2, 231: 11.7±1.8), mPrdm16 (468: 3.8±0.8, 231: 4.1±0.87), mCd137 (468: 12.2±1.8, 231: 9.2±1.2), mTbx1(468: 9.8±2.2, 231: 6.4±1.4), mMyf5 (468: 1.7±0.02, 231: 1.2±0.02), mEva1(468: 1.3±0.2, 231: 1.1±0.3), mOplah (468: 1.6±0.3, 231: 1.4±0.1), were elevated in xenografts (5 week) from MDA-MB-468, and MDA-MB-231 breast cancer cell lines (Fig. 5E and 5J). A time course experiment with the xenografts that were allowed to grow for 3, 5 or 15 weeks was performed to examine the dynamics of beige and brown adipocyte-specific proteins during xenograft development. We found UCP1, PRDM16, Myf5 and CD137 protein levels exhibited a similar temporal regulation (Fig. 5F, 5K) as observed in the original HMLE^{HRASV12} xenografts (Fig. 2D). These experiments show an increased expression of genes characteristic of beige and brown adipose in xenografts from breast cancer cell lines.

Patient-derived xenografts (PDX) exhibit beige/brown adipocyte characteristics

PDX models recapitulate tumor histology and genomic features more faithfully compared to the traditional breast cancer cell line-initiated xenografts. To evaluate whether beige/brown adipocytes are involved in primary human breast tumor development, we generated PDX by implanting subcutaneously (posterior dorsoventral side) pieces (2–3mm) of fresh tumors in nude mice. From a total of 17 primary patient-derived tumor implantations, three xenografts were established (Supplementary Table 2). All 3 PDX (PDX1, PDX2 PDX3) after 3–7months of growth (~0.5 cm in diameter) were excised, fixed with glutaraldehyde, and post-fixed with osmium. Systematic analysis of these xenografts revealed presence of typical multi-locular lipid-droplet-filled cells, characteristics of beige/brown adipocytes (Fig. 6A).

We further analyzed PDX2 for contributions from tumor cells and host in increasing the beige/brown adipocytes. We found that when compared to the original tumor pieces before implantation, there was increase in hUCP1 (4.3±1.2 fold), hCD137 (3.7±1.2 fold), hTBX1 (4.5±0.6 fold) and hMYF5 (1.6±0.1 fold). In addition, compared to the control host tissue at the site of implantation, there was increase in mUcp1 (7.4±2.3 fold), mCd137 (10.2±3.2 fold), mTbx1 (12.0±1.2 fold) and mMyf5 (2.1±0.1 fold) (Fig. 6B). Furthermore, western blot analysis showed increased expression of UCP1 in all the PDX, while CD137 was detectable only in PDX1 and PDX2 (Fig. 6C).

Moreover, immunoblot analysis of 59 human breast tumor samples showed that the majority (74.5%) had detectable UCP1 protein levels (Supplementary Table 3) (Fig. 6D). Representative pictures of different subtypes of human breast tumors immunolabelled with UCP1 antibody are shown (Fig. 6E). Collectively our data suggests expression of beige/brown adipose markers in xenografts could influence breast tumor development and could provide a rationale target for therapeutic interventions (Fig. 6F).

Discussion

Mammary gland is a dynamic heterogeneous adipose rich organ that could serve as a fertile ground for the development of breast cancer (34). Plastic properties of adipose tissue are evident in the recent identification of a third type of adipocyte, the pink adipocytes, in the subcutaneous fat depots of mice during pregnancy and lactation (35). BAT secrete a variety of adipokines, express high levels of glucose transporter-4 (GLUT4), and consume significantly higher levels of glucose (36). Using ^{18}F-fluorodeoxyglucose (FDG) tracer and PET/CT imaging, a high prevalence of BAT activity was recently found in breast cancer patients when compared to weight-matched patients with other solid tumor malignancies (12). In addition, persistent deposition of brown adipocytes has been detected in the mammary glands of BRCA1 mutant mice (13). Increased BAT in the mammary glands of these mutant mice has been correlated with up-regulation of the angiogenic marker CD31 (13). Also, a recent study shows a higher browning of mammary fat close to malignant breast tumors when compared to those in the vicinity of benign lesions (37). There is also report that white-to-brown transdifferentiation of omental adipocytes has been found in patients affected by pheochromocytoma (38).

In order to identify key adipocyte characteristics that may promote breast tumor development, we systematically analyzed xenografts obtained from various stages of tumor growth. Our study shows, for the first time to our knowledge, increase of beige and brown adipose markers in xenografts from three established breast cancer cell lines and in patient-derived xenografts. In this study, we present that multiple line of evidences obtained from our experimental findings demonstrate the increased expression of key markers for beige/brown adipose during breast tumor development. We further show the involvement of both the host as well as tumor cells in the increased expression of beige and brown adipose in the xenografts. Notably, this increase of beige and brown adipose markers from the tumor cells as well as the host was independent of the site of implantation of the tumor cells. Although expression of UCP1 has been mainly reported in beige/brown adipose tissues, its expression

has also been detected in macrophages (39), pancreas (40) and nervous tissues of torpid animals (41).

Fate of mammary epithelium, which sits in a complex niche, depends on signals from extracellular matrix as well as systemic hormonal milieu (42). Extracellular matrix, a highly variable component of the mammary gland, is composed of proteins such as collagens, laminins, and adiponectin as well adifferentiated and undifferentiated cells of hematopoietic origins, adipocytes and fibroblasts (43). Extracellular matrix of breast tumors is also complex and key determinant of cancer progression (44). Significant amount of developmentally regulated brown adipose tissue has been found in the stromal compartment of the mammary gland (45). Using BAT-depleted mouse model, it has been reported that depletion of mammary BAT in early postnatal development induces epithelial differentiation (14). Data from our study suggests that depletion of UCP1 and Myf5 positive cells significantly reduces tumor growth. The precise mechanisms by which beige/brown adipocytes contribute to xenograft growth are unknown and are a subject of future investigation. There is a possibility that increase in UCP1 expressing beige/brown adipocytes promotes expansion of subsets of mammary cancer stem cells, which facilitates xenograft growth. There is a possibility that disruption of proton-motive forces by increased UCP1 expression may lead to acidic microenvironment, which has been implicated in promoting tumor growth (46, 47). In addition, accumulation of lipids in brown adipocyte-like cells may promote fatty acid metabolism and metabolic reprogramming that could influence tumor growth. It will be interesting to explore whether up regulation of beige/brown adipocytes facilitates the formation of extracellular matrix that may contribute to expansion of subsets of cancer stem cells.

MCSCs constitute a heterogeneous pool of progenitor populations that influence different stages of breast tumor development (48). Aggressive breast tumors have high MCSC content that promotes not only progression of the disease but also its recurrence and metastasis (49). As few as 500 stem cell/cancer stem cells, that express aldehyde dehydrogenase-1 (ALDH1) in aggressive human breast tumors, have been found to initiate xenograft formation in nude mice (50). However, different sub-sets of MCSCs have not been identified and characterized due to lack of specific markers. We report for the first time that in addition to an increase in ALDH1 expression, there was an expansion of a sub-set of MCSCs that expressed PRDM16 during xenograft growth from established human breast cancer cells. PRDM16 has been established as a master regulator of the brown adipocyte differentiation program (26, 51). In presence of PRDM16, $Myf5^{+}$ precursor populations acquire brown fat characteristics specific for “classical” brown adipocytes (52). On the other hand, PRDM16 can also influence the fate of $Myf5^{-}$ precursors present mostly in the white adipocytes to acquire brown-like phenotype expressing “beige-specific” markers (53). We observed significant enrichment of both classical BAT progenitors including Myf5 and Oplah, as well as the beige adipocyte-specific markers Cd137 and Tbx1 during xenograft development, suggesting that both populations increase UCP1 expression as well as contribute to breast tumor development.

It has been well demonstrated that breast tumor cells recruit BM-MSCs, hematopoietic cells including macrophages, as well as many other cell types from the host to promote its growth

(53–54). Since substantial amount of beige adipose markers of host origin was found in the xenografts, we have been examining whether they were recruited from the microenvironment or from distant sites of the host. After extensive analysis of many adipose depots from the host, both at the site of implantation of the tumor cells as well as from distant sites, we found higher beige adipocytes of host origin within the tumor mass. There is a possibility that beige adipocytes in the xenografts might have been recruited from a yet unidentified source in the host. Since beige adipocytes are inducible, we are also considering a possibility that their increase within the tumor mass could be due to recruitment of WAT in the xenografts where they get transdifferentiated to beige adipocytes. Another possibility under consideration is that the xenografts recruit progenitors of beige adipocytes, which are usually $Myf5^{-}$ precursors, known to reside in the vicinity of WAT and induce their differentiation. A large number of inducers of beige adipocytes including cytokines, adipokines, M2 macrophages, BMP4 and BMP7 have been reported (55). Examining specific inducers that contribute to the increase of beige adipocytes could enhance our understanding of the disease for effective therapeutic interventions. In addition to the host, the tumor cells themselves contributed to the increase in beige adipose markers found in the xenografts. The fold increase of the beige adipose markers from the tumor cells appeared modest because of high basal levels from which the fold changes in the xenograft were calculated.

Our study also provides evidence that beige adipocytes could play a role in breast tumor development. Cyclooxygenase-2 (COX-2) is a rate-limiting enzyme in prostaglandin synthesis, and promotes breast cancer progression spanning pre-malignant phenotype to clinical metastasis (56). Epidemiological evidence suggests that incidence of many cancers including those in the breast is inversely related to the use of aspirin and nonsteroidal anti-inflammatory drugs, which non-specifically inhibit cyclooxygenases (57). More recently COX-2, which is a downstream effector of β-adrenergic receptor (AR) signaling in WAT, has been found to stimulate the induction of BAT in WAT depots (33). In our study, treatment of cells with BADM *in vitro* induced beige adipocyte characteristics, and larger xenografts in vivo. Also, inhibition of COX-2 but not COX-1 reduced the levels of UCP1 and PRDM16, as well as tumor size. We found brown adipocyte characteristics in our PDX model of human breast tumors, suggesting that they may contribute to human breast tumor development. Our work may explain why inhibition of β-AR/COX-2 signaling has previously been shown to suppress tumor growth in preclinical models (58). Understanding key signaling pathways in beige/brown adipocytes that contribute to breast tumor progression will enable us to develop a novel therapeutic strategy to control breast tumor development. Manipulation of browning, therefore, represents a novel strategy to inhibit tumor development.

Supplementary Material

Refer to Web version on PubMed Central for supplementary material.

Acknowledgments

Grant Support and Acknowledgements

We acknowledge Dr. Robert Weinberg (Whitehead Institute, Cambridge, MA) for HMLE^{HRASV12}cells and Dr. Srinivasa T. Reddy (UCLA School of Medicine, CA) for providing cyclooxygenase inhibitors. Fresh and frozen breast tumor specimen and sections were obtained from Cooperative Human Tissue Network (CHTN), and National Disease Research Interchange (NDRI). We gratefully appreciate the help of Michael W. Yeh, Avital Harari, Jennifer Isorena, Harold S. Sacks and Graeme Davis who participate in the human peri-adrenal adipose tissue collection or RNA isolation (IRB#13-001332-CR-00001). This work was supported by NCI SC1CA165865 (SP) and NIA SC1AG049682 (RS) grants. We also acknowledge partial supports from NIMHD U54MD007598, UCLA CTSI Grant UL1TR000124 (SP), NHLBI HL028481, and NCRR S10RR026744 (KR), and the Leducq Foundation (LV and KR).

Abbreviations

MCSC	mammary cancer stem cells
UCP1	uncoupling protein 1
COX-2	cyclooxygenase-2
BAT	brown adipose tissue
CAA	cancer-associated adipocytes
EMT	epithelial mesenchymal transition
ALDH1	aldehyde dehydrogenase 1
PRDM16	PR-domain containing 16
OCR	oxygen consumption rate
β2-AR	adrenergic receptor beta 2
β3-AR	adrenergic receptor beta 3
NDRI	National Disease Research Interchange
AA	African American
CA	Caucasian ER, Estrogen Receptor
PR	Progesterone Receptor
Her2	human epidermal growth factor receptor 2
HMLE	human mammary epithelial cells
BADM	brown adipocyte differentiation medium

References

1. Holt K. It does matter: breast cancer is the second leading cause of cancer deaths in American women (American Cancer Society, 2008). Assuming an average life span of 85 years, one in eight U.S. women will be diagnosed with breast cancer. Nurs Womens Health. 2010; 14:34–41. [PubMed: 20137041]
2. Pece S, Tosoni D, Confalonieri S, Mazzarol G, Vecchi M, Ronzoni S, Bernard L, Viale G, Pelicci PG, Di Fiore PP. Biological and molecular heterogeneity of breast cancers correlates with their cancer stem cell content. Cell. 2010; 140:62–73. [PubMed: 20074520]
3. Tan J, Buache E, Chenard MP, Dali-Youcef N, Rio MC. Adipocyte is a non-trivial, dynamic partner of breast cancer cells. Int J Dev Biol. 2011; 55:851–59. [PubMed: 21948738]
4. Zhao M, Sachs PC, Wang X, Dumur CI, Idowu MO, Robila V, Francis MP, Ware J, Beckman M, Rizki A, Holt SE, Elmore LW. Mesenchymal stem cells in mammary adipose tissue stimulate

progression of breast cancer resembling the basal-type. Cancer Biol Ther. 2012; 13:782–92. [PubMed: 22669576]

5. Nieman KM, Kenny HA, Penicka CV, Ladanyl A, Buell-Gutbrod R, Zillhardt MR, Romero IL, Carey MS, Mills GB, Hotamisligil GS, Yamada SD, Peter ME, Gwin K, Lengyel E. Adipocytes promote ovarian cancer metastasis and provide energy for rapid tumor growth. Nat Med. 2011; 17(11):1498–503. [PubMed: 22037646]
6. Dirat B, Bochet L, Dabek M, Daviaud D, Dauvillier S, Majed B, Wang YY, Meulle A, Salles B, Le Gonidec S, Garrido I, Escourrou G, Valet P, Muller C. Cancer-associated adipocytes exhibit an activated phenotype and contribute to breast cancer invasion. Cancer Res. 2011; 71:2455–65. [PubMed: 21459803]
7. Bochet L, Lehuédé C, Dauvillier S, Wang YY, Dirat B, Laurent V, Dray C, Guiet R, Maridonneau-Parini I, Le Gonidec S, Couderc B, Escourrou G, Valet P, Muller C. Adipocyte-derived fibroblasts promote tumor progression and contribute to the desmoplastic reaction in breast cancer. Cancer Res. 2013; 73:5657–68. [PubMed: 23903958]
8. Lapeire L, Hendrix A, Lambein K, Van Bockstal M, Braems G, Van Den Broecke R, Limame R, Mestdagh P, Vandesompele J, Vanhove C, Maynard D, Lehuédé C, Muller C, Valet P, Gespach CP, Bracke M, Cocquyt V, Denys H, De Wever O. Cancer-associated adipose tissue promotes breast cancer progression by paracrine oncostatin M and Jak/STAT3 signaling. Cancer Res. 2014; 74:6806–19. [PubMed: 25252914]
9. Zhao M, Dumur CI, Holt SE, Beckman MJ, Elmore LW. Multipotent adipose stromal cells and breast cancer development. Think globally, act locally. Mol Carcinog. 2010; 49:923–27. [PubMed: 20842668]
10. Karnoub AE, Dash AB, Vo AP, Sullivan A, Brooks MW, Bell GW, Richardson AL, Polyak K, Tubo R, Weinberg RA. Mesenchymal stem cells within tumour stroma promote breast cancer metastasis. Nature. 2007; 449:557–63. [PubMed: 17914389]
11. Devarajan E, Song YH, Krishnappa S, Alt E. Epithelial-mesenchymal transition in breast cancer lines is mediated through PDGF-D released by tissue-resident stem cells. Int J Cancer. 2012; 131:1023–31. [PubMed: 22038895]
12. Cao Q, Hersl J, La H, Smith M, Jenkins J, Goloubeva O, Dilsizian V, Tkaczuk K, Chen W, Jones L. A pilot study of FDG PET/CT detects a link between brown adipose tissue and breast cancer. BMC Cancer. 2014; 14:126. [PubMed: 24564204]
13. Jones LP, Buelto D, Tago E, Owusu-Boaitey KE. Abnormal Mammary Adipose Tissue Environment of Brca1 Mutant Mice Show a Persistent Deposition of Highly Vascularized Multilocular Adipocytes. J Cancer Sci Ther. 2011; (Suppl 2) pii: 004.
14. Gouon-Evans V, Pollard JW. Unexpected deposition of brown fat in mammary gland during postnatal development. Mol Endocrinol. 2002; 16:2618–27. [PubMed: 12403850]
15. Elenbaas B, Spirio L, Koerner F, Fleming MD, Zimonjic DB, Donaher JL, Popescu NC, Hahn WC, Weinberg RA. Human breast cancer cells generated by oncogenic transformation of primary mammary epithelial cells. Genes Dev. 2001; 15:50–65. [PubMed: 11156605]
16. Pervin S1, Singh R, Freije WA, Chaudhuri G. MKP-1-induced dephosphorylation of extracellular signal-regulated kinase is essential for triggering nitric oxide-induced apoptosis in human breast cancer cell lines: implications in breast cancer. Cancer Res. 2003; 63:8853–60. [PubMed: 14695202]
17. Pervin S, Tran L, Urman R, Braga M, Parveen M, Li SA, Chaudhuri G, Singh R. Oxidative stress specifically down regulates survivin to promote breast tumour formation. Br J Cancer. 2013; 108:848–58. [PubMed: 23403820]
18. Pervin S, Hewison M, Braga M, Tran L, Chun R, Karam A, Chaudhuri G, Norris K, Singh R. Down-regulation of vitamin D receptor in mammospheres: implications for vitamin D resistance in breast cancer and potential for combination therapy. PLoS One. 2013; 8:e53287. [PubMed: 23341935]
19. Kurth T, Weiche S, Vorkel D, Kretschmar S, Menge A. Histology of plastic embedded amphibian embryos and larvae. Genesis. 2012; 50:235–250. [PubMed: 22083609]

20. Petushi S, Garcia FU, Haber MM, Katsinis C, Tozeren A. Large-scale computations on histology images reveal grade-differentiating parameters for breast cancer. BMC Med Imaging. 2006; 6:14. [PubMed: 17069651]
21. Braga M, Bhasin S, Jasuja R, Pervin S, Singh R. Testosterone inhibits transforming growth factor-β signaling during myogenic differentiation and proliferation of mouse satellite cells: potential role of follistatin in mediating testosterone action. Mol Cell Endocrinol. 2012; 350:39–52. [PubMed: 22138414]
22. Braga M, Pervin S, Norris K, Bhasin S, Singh R. Inhibition of in vitro and in vivo brown fat differentiation program by myostatin. Obesity (Silver Spring). 2013; 21:1180–8. [PubMed: 23868854]
23. Braga M, Reddy ST, Vergnes L, Pervin S, Grijalva V, Stout D, David J, Li X, Tomasian V, Reid CB, Norris KC, Devaskar SU, Reue K, Singh R. Follistatin promotes adipocyte differentiation, browning, and energy metabolism. J Lipid Res. 2014; 55:375–84. [PubMed: 24443561]
24. Villanueva CJ, Vergnes L, Wang J, Drew BG, Hong C, Tu Y, Hu Y, Peng X, Xu F, Saez E, Wroblewski K, Hevener AL, Reue K, Fong LG, Young SG, Tontonoz P. Adipose subtype-selective recruitment of TLE3 or Prdm16 by PPARγ specifies lipid storage versus thermogenic gene programs. Cell Metab. 2013; 17:423–35. [PubMed: 23473036]
25. Herron D, Rehnmark S, Néchad M, Loncar D, Cannon B, Nedergaard J. Norepinephrine-induced synthesis of the uncoupling protein thermogenin (UCP) and its mitochondrial targeting in brown adipocytes differentiated in culture. FEBS Lett. 1990; 268:296–300. [PubMed: 2116978]
26. Seale P, Kajimura S, Yang W, Chin S, Rohas LM, Uldry M, Tavernier G, Langin D, Spiegelman BM. Transcriptional control of brown fat determination by PRDM16. Cell Metab. 2007; 6:38–54. [PubMed: 17618855]
27. Uldry M, Yang W, St-Pierre J, Lin J, Seale P, Spiegelman BM. Complementary action of the PGC-1 coactivators in mitochondrial biogenesis and brown fat differentiation. Cell Metab. 2006; 3:333–41. [PubMed: 16679291]
28. Wu J, Boström P, Sparks LM, Ye L, Choi JH, Giang AH, Khandekar M, Virtanen KA, Nuutila P, Schaart G, Huang K, Tu H, van Marken Lichtenbelt WD, Hoeks J, Enerbäck S, Schrauwen P, Spiegelman BM. Beige adipocytes are a distinct type of thermogenic fat cell in mouse and human. Cell. 2012; 150:366–76. [PubMed: 22796012]
29. Taube JH, Herschkowitz JI, Komurov K, Zhou AY, Gupta S, Yang J, Hartwell K, Onder TT, Gupta PB, Evans KW, Hollier BG, Ram PT, Lander ES, Rosen JM, Weinberg RA, Mani SA. Core epithelial-to-mesenchymal transition interactome gene-expression signature is associated with claudin-low and metaplastic breast cancer subtypes. Proc Natl Acad Sci U S A. 2010; 107(35): 15449–54. [PubMed: 20713713]
30. Curran CS, Keely PJ. Breast tumor and stromal cell responses to TGF-β and hypoxia in matrix deposition. Matrix Biol. 2013; 32:95–105. [PubMed: 23262216]
31. Ricquier D, Nechad M, Mory G. Ultrastructural and biochemical characterization of human brown adipose tissue in pheochromocytoma. J Clin Endocrinol Metab. 1982; 54:803–7. [PubMed: 7061689]
32. Liu S, MS. Targeting breast cancer stem cells. J Clin Oncol. 2010; 28:4006–12. [PubMed: 20498387]
33. Vegiopoulos A, Müller-Decker K, Strzoda D, Schmitt I, Chichelnitskiy E, Ostertag A, Berriel Diaz M, Rozman J, Hrabe de Angelis M, Nüsing RM, Meyer CW, Wahli W, Klingenspor M, Herzig S. Cyclooxygenase-2 controls energy homeostasis in mice by de novo recruitment of brown adipocytes. Science. 2010; 328:1158–61. [PubMed: 20448152]
34. Hovey RC, Aimo L. Diverse and active roles for adipocytes during mammary gland growth and function. J Mammary Gland Biol Neoplasia. 2010; 15:279–90. [PubMed: 20717712]
35. Giordano A, Smorlesi A, Frontini A, Barbatelli G, Cinti S. White, brown and pink adipocytes: the extraordinary plasticity of the adipose organ. Eur J Endocrinol. 2014; 170:R159–71. [PubMed: 24468979]
36. Orava J, Nuutila P, Lidell ME, Oikonen V, Noponen T, Viljanen T, Scheinin M, Taittonen M, Niemi T, Enerbäck S, Virtanen KA. Different metabolic responses of human brown adipose tissue to activation by cold and insulin. Cell Metab. 2011; 14:272–9. [PubMed: 21803297]

37. Wang F, Gao S, Chen F, Fu Z, Yin H, Lu X, Yu J, Lu C. Mammary fat of breast cancer: Gene expression profiling and functional characterization. PLoS One. 2014; 9:e109742. [PubMed: 25291184]
38. Frontini A, Vitali A, Perugini J, Murano I, Romiti C, Ricquier D, Guerrieri Cinti S. White-to-brown transdifferentiation of omental adipocytes in patients affected by pheochromocytoma. Biochem Biophy Acta. 2013:950–959.
39. Gundra UM, Girgis NM, Ruckerl D, Jenkins S, Ward LN, Kurtz ZD, Wiens KE, Tang MS, Basu-Roy U, Mansukhani A, Allen JE, Loke P. Alternatively activated macrophages derived from monocytes and tissue macrophages are phenotypically and functionally distinct. Blood. 2014; 123(20):e110–22. [PubMed: 24695852]
40. Sale MM, Hsu FC, Palmer ND, Gordon CJ, Keene KL, Borgerink HM, Sharma AJ, Bergman RN, Taylor KD, Saad MF, Norris JM. The uncoupling protein 1 gene, UCP1, is expressed in mammalian islet cells and associated with acute insulin response to glucose in African American families from the IRAS Family Study. BMC Endocr Disord. 2007; 7:1. [PubMed: 17397545]
41. Laursen WJ, Mastrotto M, Pesta D, Funk OH, Goodman JB, Merriman DK, Ingolia N, Shulman GI, Bagriantsev SN, Gracheva EO. Neuronal UCP1 expression suggests a mechanism for local thermogenesis during hibernation. Proc Natl Acad Sci U S A. 2015; 112(5):1607–12. [PubMed: 25605929]
42. Oakes SR, Gallego-Ortega D, Ormandy CJ. The mammary cellular hierarchy and breast cancer. Cell Mol Life Sci. 2014; 22:4301–24. [PubMed: 25080108]
43. Oskarsson T. Extracellular matrix components in breast cancer progression and metastasis. The Breast. 2013; 22:S66–S72. [PubMed: 24074795]
44. Naba A, Clauser KR, Lamar JM, Carr SA, Hynes RO. Extracellular matrix signatures of human mammary carcinoma identify novel metastasis promoters. Elife. 2014; 11(3):e01308. [PubMed: 24618895]
45. Master SR, Hartman JL, D'Cruz CM, Moody SE, Keiper EA, Ha SI, Cox JD, Belka GK, Chodosh LA. Functional microarray analysis of mammary organogenesis reveals a developmental role in adaptive thermogenesis. Mol Endocrinol. 2002; 16:1185–1203. [PubMed: 12040007]
46. Rofstad EK, Mathiesen B, Kindem K, Galappathi K. Acidic extracellular pH promotes experimental metastasis of human melanoma cells in athymic nude mice. Cancer Res. 2006; 66(13):6699–707. [PubMed: 16818644]
47. Kato Y, Ozawa S, Miyamoto C, Maehata Y, Suzuki A, Maeda T, Baba Y. Acidic extracellular microenvironment and cancer. Cancer Cell Int. 2013; 13(1):89.10.1186/1475-2867-13-89 [PubMed: 24004445]
48. Gupta PB, Onder TT, Jiang G, Tao K, Kuperwasser C, Weinberg RA, Lander ES. Identification of selective inhibitors of cancer stem cells by high-throughput screening. Cell. 2009; 38:645–59. [PubMed: 19682730]
49. Tsang JY, Huang YH, Luo MH, Ni YB, Chan SK, Lui PC, Yu AM, Tan PH, Tse GM. Cancer stem cell markers are associated with adverse biomarker profiles and molecular subtypes of breast cancer. Breast Cancer Res Treat. 2012; 36:407–17. [PubMed: 23053657]
50. Ginestier C, Hur MH, Charafe-Jauffret E, Monville F, Dutcher J, Brown M, Jacquemier J, Viens P, Kleer CG, Liu S, Schott A, Hayes D, Birnbaum D, Wicha MS, Dontu G. ALDH1 is a marker of normal and malignant human mammary stem cells and a predictor of poor clinical outcome. Cell Stem Cell. 2007; 1:555–67. [PubMed: 18371393]
51. Harms MJ, Ishibashi J, Wang W, Lim HW, Goyama S, Sato T, Kurokawa M, Won KJ, Seale P. Prdm16 is required for the maintenance of brown adipocyte identity and function in adult mice. Cell Metab. 2014; 19:593–604. [PubMed: 24703692]
52. Seale P, Bjork B, Yang W, Kajimura S, Chin S, Kuang S, Scimè A, Devarakonda S, Conroe HM, Erdjument-Bromage H, Tempst P, Rudnicki MA, Beier DR, Spiegelman BM. PRDM16 controls a brown fat/skeletal muscle switch. Nature. 2008; 454:961–7. [PubMed: 18719582]
53. Tawada M, Hayashi S, Ikegame Y, Nakashima S, Yoshida K. Possible involvement of tumor-producing VEGF-A in the recruitment of lymphatic endothelial progenitor cells from bone marrow. Oncol Rep. 2014; 32:2359–64. [PubMed: 25242215]

54. Santander AM, Lopez-Ocejo O, Casas O, Agostini T, Sanchez L, Lamas-Basulto E, Carrio R, Cleary MP, Gonzalez-Perez RR, Torroella-Kouri M. Paracrine Interactions between Adipocytes and Tumor Cells Recruit and Modify Macrophages to the Mammary Tumor Microenvironment: The Role of Obesity and Inflammation in Breast Adipose Tissue. Cancers (Basel). 2015; 7:143–78. [PubMed: 25599228]

55. Qian S, Huang H, Tang Q. Brown and beige fat: the metabolic function, induction, and therapeutic potential. Front Med. 2015; 9:162–72. [PubMed: 25573295]

56. Fornetti J, Jindal S, Middleton KA, Borges VF, Schedin P. Physiological COX-2 expression in breast epithelium associates with COX-2 levels in ductal carcinoma in situ and invasive breast cancer in young women. Am J Pathol. 2014; 184:1219–1229. [PubMed: 24518566]

57. Arun B, Goss P. The role of COX-2 inhibition in breast cancer treatment and prevention. Semin Oncol. 2004; 31:22–29. [PubMed: 15179621]

58. Barron TI, Connolly RM, Sharp L, Bennett K, Visvanathan K. Beta blockers and breast cancer mortality: a population-based study. J Clin Oncol. 2011; 29:2635–44. [PubMed: 21632503]

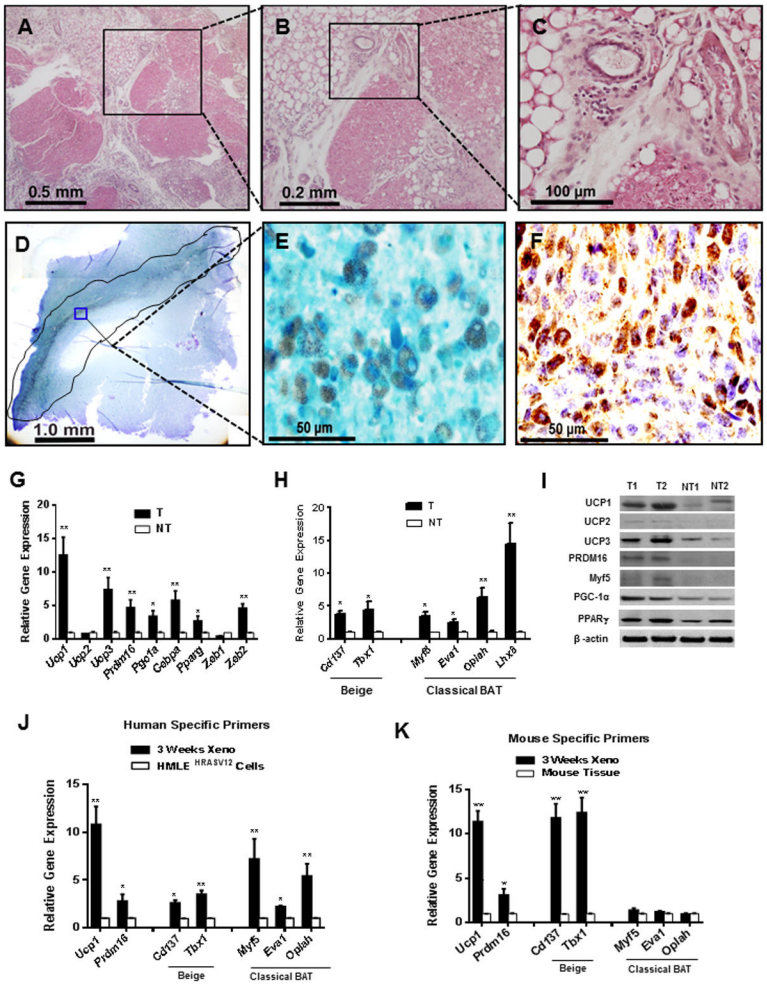

Figure 1.

Transplantable HMLE^{HRASV12} xenografts show multi-locular lipid droplets and express beige/brown adipocyte-specific proteins. Cells (2×10^6) from primary HMLE^{HRASV12} xenografts were mixed with matrigel (1:1) and implanted at a subcutaneous site (posterior dorsolateral) to develop xenografts. A–C, Low and high magnification images of hematoxylin/eosin-stained sections of transplantable (T) xenografts (7–10 week). Representative data is shown from multiple experiments (n=6). D–E, Bright field low and high magnification images of T xenografts (5–7 week) that were fixed in glutaraldehyde, post-fixed with osmium tetroxide, and stained with toluidine blue, showing brown stained lipid droplets. A representative image is shown from multiple experiments (n=6). F, Immuno-labelling of paraffin embedded sections of T xenograft for UCP1 protein. G–H, Relative gene expression of beige/brown adipocyte markers from T and NT xenografts (5 week) using human-specific primers (*p<.05, **p<.01). Data are presented as mean ± SD from 4 independent experiments. I, Lysates from T and NT are analyzed for brown adipocyte specific proteins by Western blot analysis. J–K Relative gene expression of beige and brown adipocyte markers in xenografts, using human- (J) and mouse- (K) specific primers. (*p<.05, **p<.01). Basal expression in cells before implantation or mouse tissue at

the site of implantation was used to calculate relative gene expression of markers in xenografts (3 week) using human- or mouse-specific primers respectively. Data are presented as mean ± SD from 4 independent experiments.

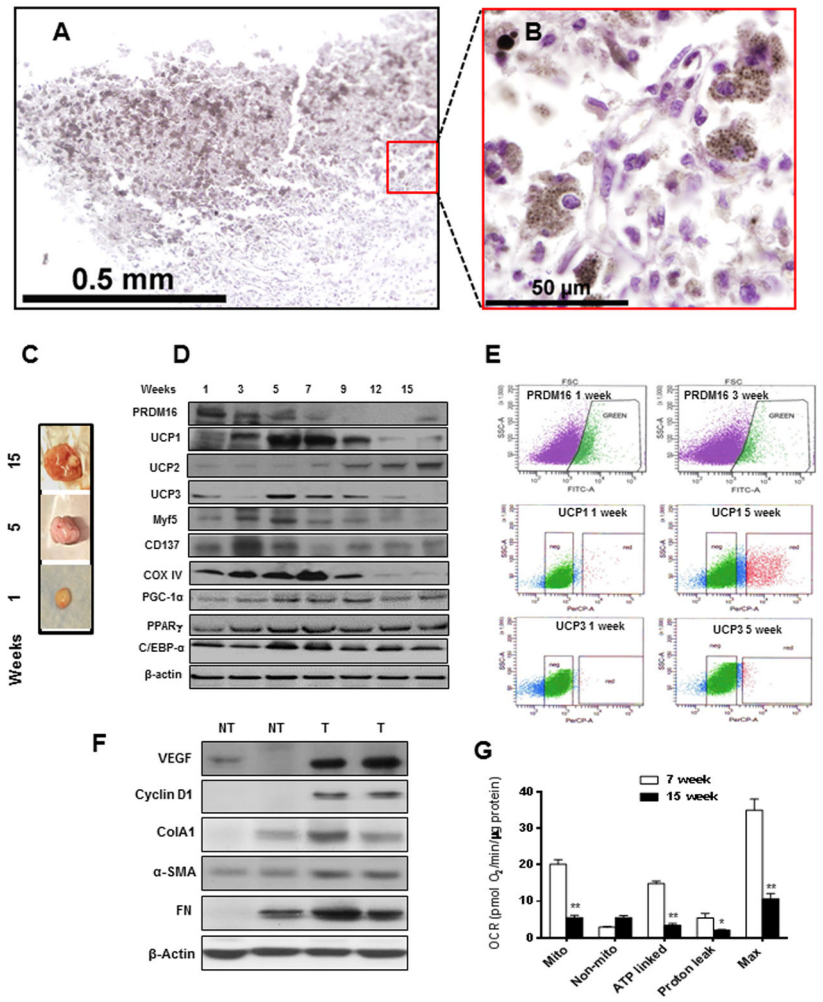

Figure 2.

Presence of cells with brown adipocyte phenotype and characteristics in HMLE^{HRASV12}xenografts over time. A–B, Xenografts at various stages of growth were fixed with glutaraldehyde, post-fixed with osmium tetroxide and embedded in Technovit. Low (A) and high (B) magnification pictures of hematoxylin/eosin-stained sections are shown. Cells (2×10^6) from a transplantable HMLE^{HRASV12} xenograft were mixed with matrigel (1:1) and implanted at a subcutaneous site (posterior dorsolateral) in nude mice to develop xenografts, which were excised at various time points. C, Representative bright field images of xenografts at 1, 5, and 15 week. D, Western blot analysis of pooled lysates (n=3 mice/time point) from xenografts excised at various time points after growth subcutaneously in nude mice. A representative western blot analysis is shown (n=3). E, FACS analysis of PRDM16 (1- and 3 week xenograft), and UCP1, and UCP3 (1- and 5 week xenograft) labeled cells. Data shown is a representation of multiple experiments (n=3). F, Western blot analysis of key markers of angiogenesis (VEGF), proliferation (cyclin D1), and extracellular matrix proteins (ColA1, SMA and FN) in NT and T xenografts. G, Analysis of cellular bioenergetics of cells (4×10^4) obtained from 7-and 15-week xenografts (n=3,*p<.05, and **p<.001). Bar graphs show mean ± SD.

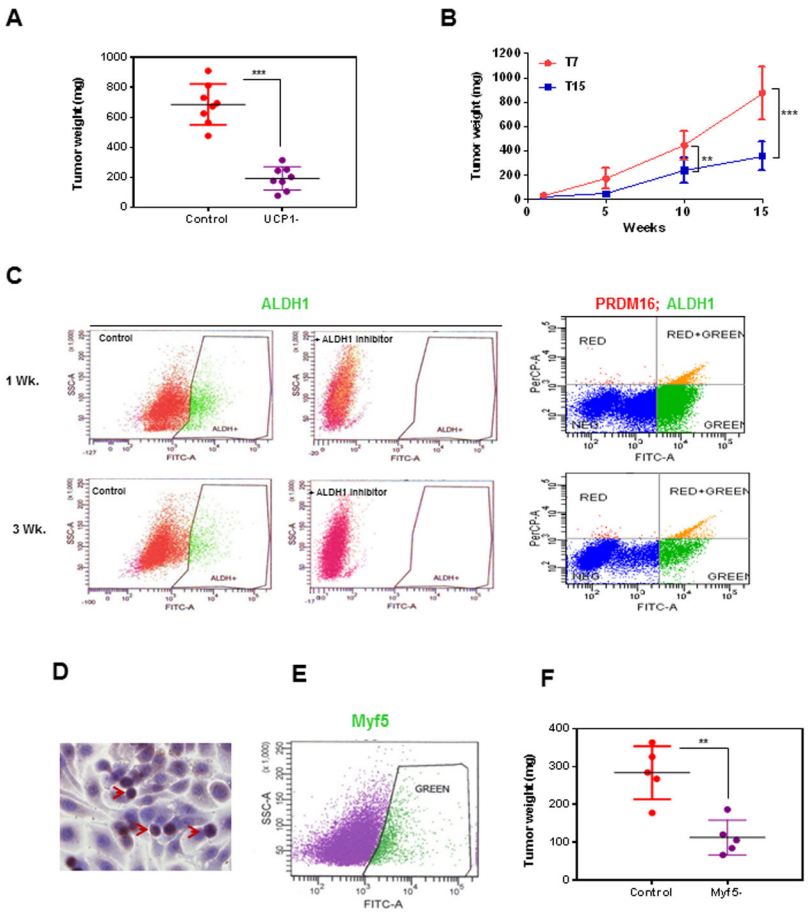

Figure 3.

Depletion of UCP1 and Myf5 population reduced xenograft growth. A, Cells (2×10^6) from primary HMLE^{HRASV12} xenografts was mixed with matrigel (1:1) and implanted at a subcutaneous site (posterior dorso-lateral) in nude mice (n=8). 5 weeks after implantation of cells, the mice were killed, tumors were excised and dissociated. Dissociated cells (2×10^7) from each of the eight xenografts were individually sorted by FACS into UCP1+ and UCP1− populations. From each of the xenografts, control unsorted (2×10^6) or UCP1$^-$ (2×10^6) fraction of the sorted cells were injected subcutaneously (posterior dorsolateral) into nude mice (n=8). After 10 weeks, the mice were killed, tumors were excised and tumor weight was measured. B, Cells (2×10^6) from 7- and 15-week xenografts were injected into nude mice (subcutaneously, posterior dorsolateral) (n=3, per group per time point). Mice were killed, xenografts were excised and weighed at each of the time points. Data are presented as mean ± SD. (*p<.05, and **p<.01). C, Cells from dissociated xenografts (1- and 3-week) were subjected to flow cytometry to determine the percentage of ALDH1 (ALDH1 Ab /FITC) as well as ALDH1/PRDM16 (ALDH1 Ab /FITC, PRDM16 Ab/Texas Red) co-expressing cells. D. Paraffin -embedded sections of xenografts were immuno-labeled for Myf5 and a representative picture is shown. Arrows show Myf5 stained cells. E, Myf5-expressing cells in the dissociated xenografts can be sorted by labeling with Myf5-FITC Abs. A representative picture is shown. F, Dissociated cells (2×10^7) from xenografts

(1–3 week) was sorted by FACS into Myf5+ and Myf5− populations. Control unsorted (2×10^6) or Myf5$^-$ (2×10^6) fraction of the sorted cells were injected subcutaneously (posterior dorsolateral) into nude mice (n=5). After 4 weeks the mice were killed, tumors were excised and tumor weight was measured. Data are presented as mean ± SD. (*p<.05, **p<.01).

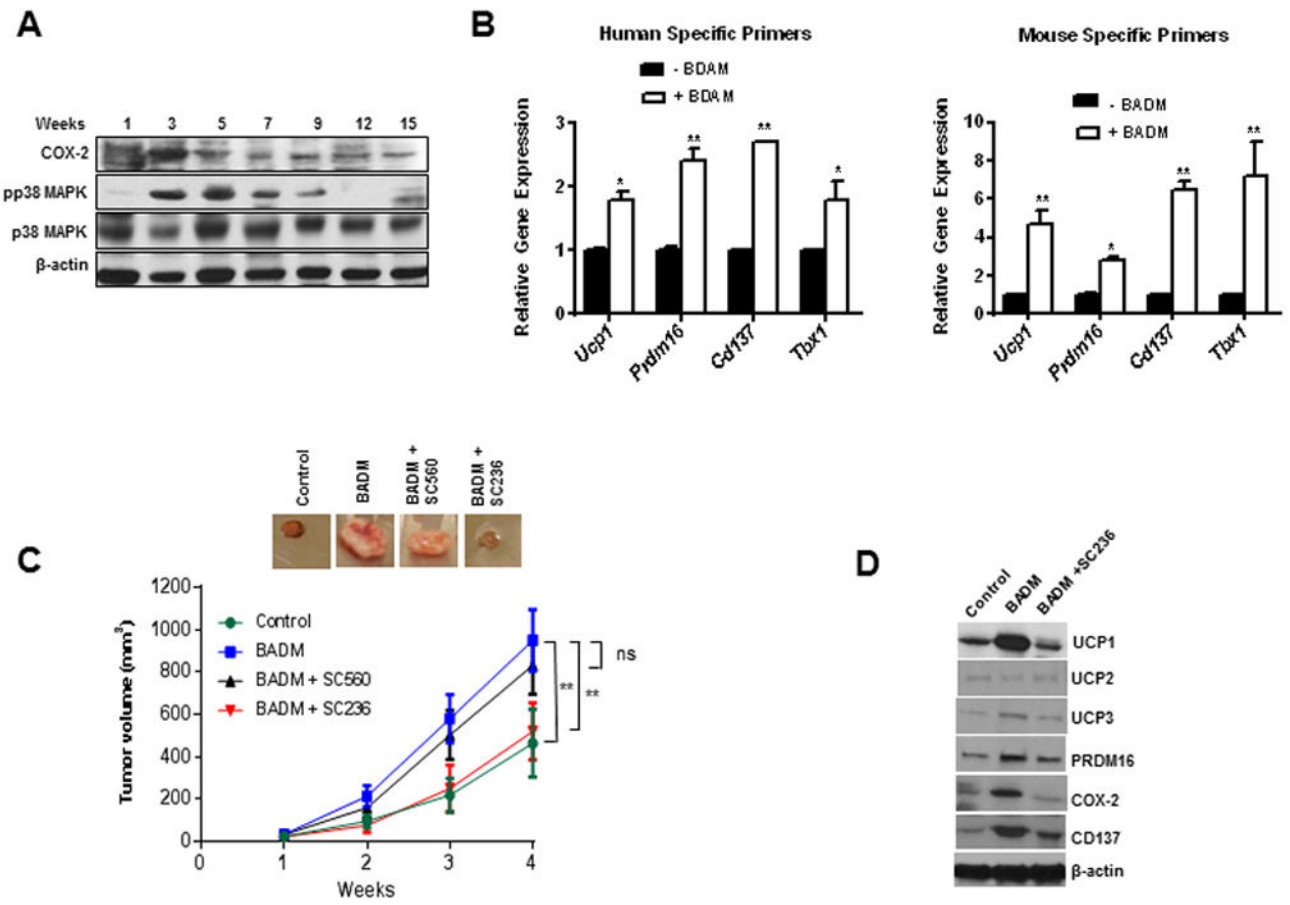

Figure 4.

Treatment of HMLE^{HRASV12} cells with brown adipocyte differentiation media promotes xenograft formation. A, Cells (2×10^6) from transplantable HMLE^{HRASV12} xenografts was mixed with matrigel (1:1) and implanted at a subcutaneous site (posterior dorso-lateral) in nude mice to develop xenografts, which were excised at various time points. Lysates (pooled from 3 separate experiments/time points) of xenografts grown for different time points were examined for COX-2 and pp38 MAP Kinase protein expression. A representative western blot analysis is shown. B, HMLE^{HRASV12} cells treated with (+BADM) or without (−BADM) differentiation media for 48h were injected (2×10^6 cells) subcutaneously (posterior dorsolateral). Mice (n=3 mice/group) were killed after two weeks, RNA was extracted from the xenografts, quantitative PCR of beige and brown markers was performed using human (B, left panel) as well as mouse (B, right panel) specific primers. Relative gene expression levels in BADM-induced xenografts were calculated relative to the control (−BADM) group. Data are presented as mean ± SD. (*p<.05, **p<.01). C, Control (−BADM) or BADM-induced cells (induced for 48hr) were further treated with or without COX inhibitors (SC560: 10nM; SC236: 10nM) for 24h before they were injected (2×10^6 cells) in mice (n=5 mice per group) and tumor volumes were measured between 1–4 week (**p<.01), ns, none significant. D, Lysates of xenografts (2 week) from control (−BADM), BADM and BADM + SC236 treated groups were examined for various proteins by western blot.

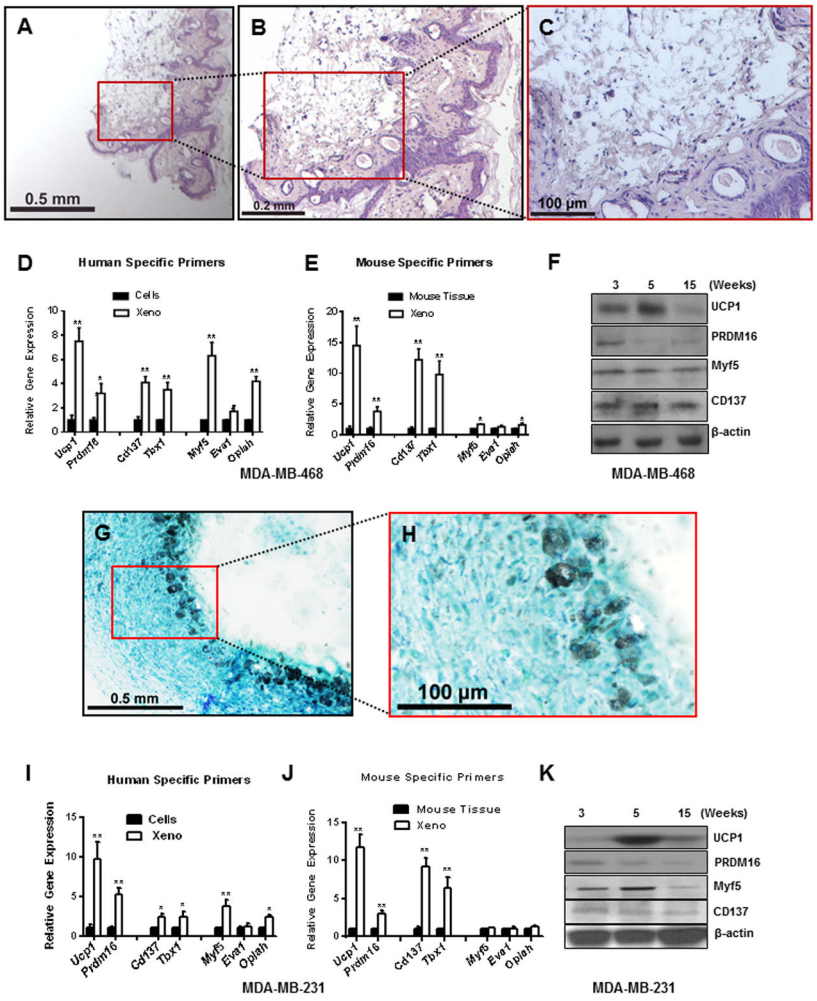

Figure 5.

Increase in beige/brown adipocyte characteristics in the xenografts from additional breast cancer cell lines. Breast cancer cells (2×10^6 cells), purchased from ATCC, were propagated in their respective media, mixed with matrigel and implanted subcutaneously (posterior, dorsolateral) in nude mice (n=5 mice per cell line). A–C, Hematoxylin/Eosin-stained picture of xenograft sections obtained from MDA-MB-468 cells. A representative picture at low (5A) and high magnifications (B,C) is shown. D–E, Quantitative real-time PCR analysis using human and mouse-specific primers in xenografts (5 week) from MDA-MB-468 cells. Relative expression levels in the xenografts were compared either to the cells before implantation (human-specific primers) or with mouse tissue at the site of implantation (mouse-specific primers). Data are shown as mean ± SD, (n=4). F, MDA-MB-468 cells (2×10^6) were mixed with matrigel and subcutaneously implanted in mice. Mice were killed at different time points and tissue lysates from excised tumors were analyzed by western blot for different beige/brown-specific proteins. (n=3 mice per time point). Pooled samples from each time point were analyzed by western blot analysis. G–H Representative bright field picture of xenograft sections obtained from MDA-MB-231 cells, toluidine blue stain. I–J, Quantitative real-time PCR analysis of xenografts obtained after 5 week of implantation

of MDA-MB-231 cells compared either to the cells before implantation (human-specific primers) or with mouse tissue at the site of implantation (mouse-specific primers). Data are shown as mean ± SD, (n=4). K, MDA-MB-231 cells (2×10^{6}) were mixed with matrigel and subcutaneously implanted in mice. Mice were killed at different time points and tissue lysates from excised tumors were analyzed by western blot for different beige/brown specific proteins. (n=3 mice per time point). Pooled samples from each time point were analyzed by western blot analysis.

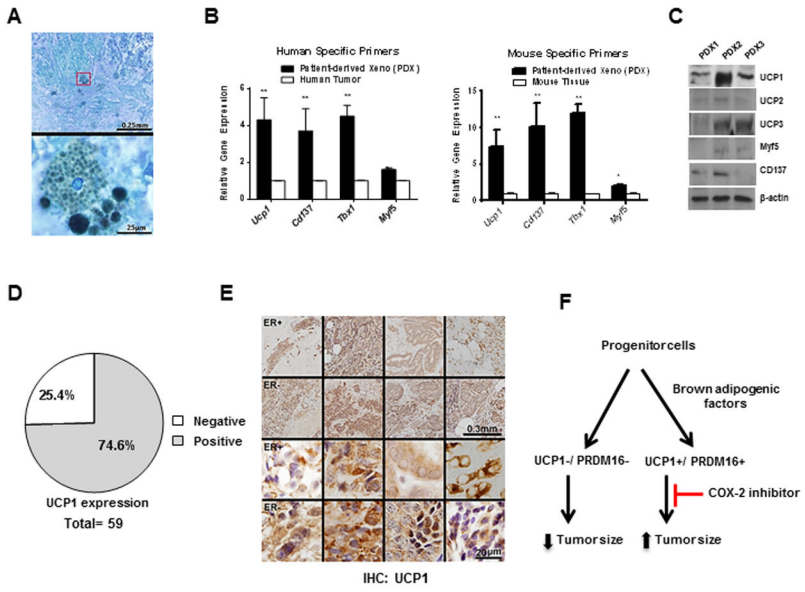

Figure 6.

A, Presence of multi-locular lipid droplets in patient-derived xenografts (PDX), toluidine blue stain. Fresh human tumors were chopped to 1–2 mm in diameter, mixed with matrigel, implanted subcutaneously (posterior dorsolateral) and allowed to grow till it reaches a diameter of 0.5 cm after which the mice were killed and the PDX was excised. Only 3 PDX (PDX1, PDX2, and PDX3) were generated within a course of 3–7 months (Supplementary Table 2). Each of the 3 PDX was fixed in glutaraldehyde and post-fixed with osmium tetroxide sectioned, and stained with toluidine blue and analyzed. A, A representative image is shown. B, RNA was extracted from each of the three PDX as well as the original human tumor before implantation. Quantitative PCR analysis of beige/brown related markers using human-specific (B, left panel), as well as mouse-specific (B, right panel) primers was performed. Fold changes in the expression of respective genes relative to the tumors before implantation was calculated and mean ± SD for all PDX was shown (*p<.05, **p<.01). C, Western blot analysis of PDX-lysates was analyzed for various beige/brown related proteins. D, Pictogram showing a summary of UCP1 protein expression examined by Western blot analysis from 59 human breast tumor specimens as listed in Supplementary Table 3. E. Paraffin embedded sections of human breast tumors was immunolabeled for UCP1 and representative images of estrogen receptor positive (ER^+) and negative (ER^-) tumor sections are shown. F, A representative model suggesting the role of $UCP1^+/PRDM16^+$ population during tumor development.